GeV emission from gamma-ray bursts: a radiative fireball?

G. Ghisellini,[1][*] G. Ghirlanda,[2] L. Nava[1,2] and A. Celotti[2]

[1]*INAF – Osservatorio Astronomico di Brera, via E. Bianchi 46, I-23807 Merate, Italy*
[2]*SISSA, via Beirut 2–4, I-34014 Trieste, Italy*

ABSTRACT

We study the emission observed at energies >100 MeV of 11 gamma-ray bursts (GRBs) detected by the *Fermi*–Large Area Telescope (LAT) until 2009 October. The GeV emission has three main properties: (i) its duration is often longer than the duration of the softer emission detected by the Gamma Burst Monitor onboard *Fermi* (this confirms earlier results from the Energetic Gamma-Ray Experiment Telescope); (ii) its spectrum is consistent with $F_\nu \propto \nu^{-1}$ and does not show strong spectral evolution; and (iii) for the brightest bursts the flux detected by the LAT decays as a power law with a typical slope $t^{-1.5}$. We argue that the observed >0.1 GeV flux can be interpreted as afterglow emission shortly following the start of the prompt phase emission as seen at smaller frequencies. The decay slope is what is expected if the fireball emission is produced in the radiative regime, i.e. all dissipated energy is radiated away. We also argue that the detectability in the GeV energy range depends on the bulk Lorentz factor Γ of the bursts, being strongly favoured in the case of large Γ. This implies that the fraction of bursts detected at high energies corresponds to the fraction of bursts having the largest Γ. The radiative interpretation can help to explain why the observed X-ray and optical afterglow energetics are much smaller than the energetics emitted during the prompt phase, despite the fact that the collision with the external medium should be more efficient than internal shocks in producing the radiation that we see.

Key words: radiation mechanisms: non-thermal – gamma-rays: bursts – gamma-rays: theory – X-rays: general.

1 INTRODUCTION

The *Fermi Gamma Ray Space Telescope* (*Fermi*) has onboard two instruments: the Large Area Telescope (LAT), sensitive in the 100 MeV–100 GeV energy range (and even beyond 100 GeV, for very bright sources; Atwood et al. 2009), and the Gamma Burst Monitor (GBM), especially designed for the detection of gamma-ray bursts (GRBs), sensitive in the 8 keV–40 MeV energy range (Meegan et al. 2009). The LAT revealed 12 GRBs above 100 MeV confirming that GRBs can be sources of very high-energy photons and that the fraction of GRBs that can be detected at these energies is roughly 10 per cent of those detected by the GBM at lower energies. It was the Energetic Gamma-Ray Experiment Telescope (EGRET) instrument, onboard the *Compton Gamma Ray Observatory* (*CGRO*) that was the first to detect GRBs above 100 MeV (Fishman & Meegan 1995; Kaneko et al. 2008), but it is the much better sensitivity (and reduced dead time) of the LAT that allows us for the first time to try to understand the origin of this emission and to answer the question: does it belong to the prompt phase or

is it afterglow emission produced by the fireball colliding with the circumburst medium? Or has it still another origin?

One of the puzzling features of the high-energy emission as revealed by EGRET was that it was long lasting, yet it started during the prompt phase as seen by the Burst Alert and Transient Source Experiment (BATSE) onboard *CGRO* and sensitive in the 30 keV–1 MeV energy band. For instance, GRB 940217 emitted >100 MeV photons up to 1.5 h after the prompt phase ended in the BATSE detector. A photon of 18 GeV was received ∼5000 s after the trigger (Hurley et al. 1994), and this was the highest photon energy of a GRB until the *Fermi*–LAT era. On the other hand, about a third of the high-energy photons were received within 120 s, before the end of the prompt phase as detected by BATSE.

Up to now, there have been three LAT-detected GRBs already discussed in the literature. In GRB 080916C (Abdo et al. 2009a), there is evidence that the spectrum from 8 keV to 10 GeV can be described by the same Band function (i.e. two smoothly connected power laws), suggesting that the LAT flux has the same origin of the low-energy flux. On the other hand, the flux level of the LAT emission, its spectrum and its long-lasting nature match the expectations from a forward shock, leading Kumar & Barniol-Duran (2009) to prefer the 'standard afterglow' interpretation [see also

[*]E-mail: gabriele.ghisellini@brera.inaf.it

Table 1. The 12 bursts detected by the *Fermi*–LAT instrument above 100 MeV, until 2009 October 3.

GRB	z	T_{90} s	S_{GBM}	α_{GBM}	β_{GBM}	E_{peak} (keV)	Ref.	$E_{\gamma,iso}$ (erg)	S_{GBM} (8–10⁴ keV)	S_{LAT} (0.1–100 GeV)
080825C	–	22	2.4e–5	-0.39 ± 0.04	-2.34 ± 0.09	155 ± 5	8141	–	(3.4 ± 0.3)e–5	(9.5 ± 4)e–6
080916C	4.35	66	1.9e–4[a]	-0.91 ± 0.02	-2.08 ± 0.06	424 ± 24	8278	5.6e54	(1.6 ± 0.2)e–4	(7 ± 1)e–5
081024B	–	0.8	(3.4 ± 0.1)e–7	-0.70 ± 0.13	–	1583 ± 520	8407	–	(3.2 ± 0.1)e–6	(3 ± 2)e–6
081215	–	∼90	(2.8 ± 0.5)e–6[b]	-0.14 ± 0.26	–	139 ± 14	8682	–		
090217	–	32.8	(3.08 ± 0.03)e–05	-0.845 ± 0.023	-2.86 ± 0.3	610 ± 32	8902	–	(3.8 ± 0.4)e–5	(4.2 ± 1.6)e–6
090323	3.57	∼150	(1.00 ± 0.01)e–4	-0.89 ± 0.03	–	697 ± 51	9021	3.4e54	(1.32 ± 0.03)e–4	(3.6 ± 0.8)e–5
090328	0.736	∼25	(8.09 ± 0.10)e–5	-0.93 ± 0.02	-2.2 ± 0.1	653 ± 45	9057	2.1e53	(1.52 ± 0.02)e–4	(3.3 ± 2)e–5
090510	0.903	1	(3.0 ± 0.2)e–5[c]	-0.80 ± 0.03	-2.6 ± 0.3	4400 ± 400	9336	5.0e52	(2.3 ± 0.2)e–5	(3.7 ± 0.7)e–5
090626	–	70	(3.5 ± 0.1)e–5	-1.2 ± 0.02	-1.98 ± 0.02	175 ± 12	9579	–	(6.0 ± 0.2)e–5	(9.6 ± 6)e–6
090902B	1.822	∼21	(3.74 ± 0.03)e–4[d]	-0.696 ± 0.012	-3.85 ± 0.25	775 ± 11	9866	4.4e54	(5.4 ± 0.04)e–4	(5.9 ± 0.6)e–4
090926A	2.106	20 ± 2	(1.45 ± 0.04)e–4	-0.75 ± 0.01	-2.59 ± 0.05	314 ± 4	9933	2e54	(1.9 ± 0.05)e–4	(4.3 ± 0.8)e–5
091003	0.897	21 ± 0.5	(3.76 ± 0.04)e–5	-1.13 ± 0.01	-2.64 ± 0.24	86.2 ± 23.6	9983	8.7e52	(4.16 ± 0.03)e–5	(1.3 ± 0.8)e–5

Note. Besides their redshifts (when measured) and duration, we give the parameters of the time integrated GBM spectrum collected from the literature and the corresponding reference. Fluences S are in erg cm^{-2}, peak energies E_{peak} in keV. In column 10 we report the fluence S in the 8 keV–10 MeV energy range calculated from the spectral parameters of the GBM. Column 11 reports the fluence in the 0.1–100 GeV energy range obtained from the analysis of the LAT spectra performed in this paper (whose results are given in Table 2). We adopted a Band model for the GBM, and a simple power law of photon slope Γ for the LAT. When β is not indicated, the adopted fitting model is a cut off power-law of photon slope α. [a] S_{GBM} in the 8 keV–30 MeV energy range; [b] S_{GBM} in the 50–300 keV energy range; [c] S_{GBM} in the 50 keV–40 MeV energy range; [d] S_{GBM} in the 50 keV–10 MeV energy range. The number quoted in the 'Ref.' column refer to GCN circulars as follows: 8141 – van der Horst & Connaughton (2008); 8278 – van der Horst & Goldstein (2008); 8407 – Omodei (2008); 8682 – Chaplin, van der Horst & Preece (2008); 8902 – von Kienlin (2009a); 9021 – Ohno et al. (2009); 9057 – Rau, Connaughton & Briggs (2009); 9336 – Guiriec, Connaughton & Briggs (2009); 9579 – von Kienlin (2009b); 9866 – Bissaldi & Connaughton (2009); 9933 – Bissaldi (2009); 9983 – Rau (2009).

Razzaque, Dermer & Finke (2009) for a hadronic model; Zhang & Peer (2009) for a magnetically dominated fireball model and Zou, Fan & Piran (2009) for a synchrotron self-Compton origin].

In the short burst GRB 090510, the spectrum in the LAT energy range is not the extrapolation of the flux from lower energies, but is harder, leading Abdo et al. (2009b) to propose a synchrotron self-Compton interpretation for its origin. Instead, we (Ghirlanda, Nava & Ghisellini 2010) proposed that the LAT flux is afterglow synchrotron emission, on the basis of its time profile and spectrum (see also Gao et al. 2009; De Pasquale et al. 2009).

Finally, the LAT flux of GRB 090902B decays as $t^{-1.5}$ (Abdo et al. 2009c), it lasts longer than the flux detected by the GBM, and its spectrum is harder than the extrapolation from lower frequencies, making it a good candidate for an afterglow interpretation, despite the arguments against put forward by Abdo et al. (2009c) that we will discuss in this paper. Moreover, in GRB 090902B there is evidence of a soft excess (observed in the GBM spectrum below 50 keV) which is spectrally consistent with the extrapolation at these energies of the LAT spectrum.

As the few examples above demonstrate, there is no consensus yet on the nature of the high-energy emission of GRBs. Since only three of the nearly dozen bursts detected by the LAT have already been discussed in the literature, we present here a study of the entire sample of bursts detected at high energies by the LAT. We will construct the light curves of the high-energy flux and the spectral shape in the 0.1–100 GeV energy range, to find if there are properties that are common among different bursts that can help to understand their nature.

Indeed, we believe that a consistent scenario emerges: the LAT spectra are often inconsistent with the extrapolation of the GBM spectra (except in two cases) and the light curves can be often described by a power-law decay in time, i.e. $F_{LAT} \propto t^{-\alpha}$, with a slope often close to $\alpha = 1.5$. In the brightest cases, the rising part is also visible and is consistent with $F_{LAT} \propto t^2$. These are, in our opinion, strong indications of the afterglow nature of the

LAT emission. Furthermore, we suggest that GRBs with a flux decaying as $F_{LAT} \propto t^{-1.5}$, and with a spectral slope around unity [i.e. $F(\nu) \propto \nu^{-1}$], are emitting in the radiative regime of a forward shock. We will also point out the role that the electron–positron pair production process has in establishing the radiative regime. Finally, we will discuss the consequences of our findings.

We adopt a cosmology with $h = \Omega_\Lambda = 0.7$ and $\Omega_M = 0.3$ and the convention $Q = 10^x Q_x$, using cgs units.

2 SAMPLE AND DATA ANALYSIS

We considered all the 12 bursts detected in the *Fermi*–LAT until 2009 October 3. These are reported in Table 1 with their redshifts (column 2) and the spectral parameters and fluences (columns 4–7) as reported in the literature, obtained from the analysis of the GBM spectrum. Since the GBM fluences reported in the literature refer to different energy ranges, we convert all the GBM fluences to the common 8 keV–10 MeV energy range (column 10). In addition (last column), we report the fluences in the 0.1–100 GeV energy range of the LAT obtained from the spectral analysis of the LAT data (spectral parameters are given in Table 2). For those GRBs with measured redshifts, we computed the isotropic equivalent energy $E_{\gamma,iso}$ by integrating the GBM spectral model in the 1 keV–10 MeV rest-frame energy range.

Among the considered bursts, there are three cases which have been published in recent papers: GRB 080916C (Abdo et al. 2009a), GRB 090510 (Abdo et al. 2009b; Ghirlanda et al. 2010) and GRB 090902B (Abdo et al. 2009c). All the others are unpublished. We did not consider GRB 081215 which, lying at a large angle (86°) with respect to the LAT boresight (Preece 2008), required a non-standard analysis of the LAT data (McEnery et al. 2008). GRB 081024B and GRB 090510 are of the short class. Seven bursts have measured redshifts; for all the others we assume a typical redshift of 2 and 1 for the long and short classes.

Table 2. LAT spectral results.

GRB	t_0 (s)	t_1 (s)	Γ_{LAT}	C_{stat}/d.o.f.	Flux (erg cm^{-2} s^{-1})
080825C	0	200	1.96 ± 0.3	10/6	(4.0 ± 2.0)e–8
080916C	0	200	2.09 ± 0.12	19/15	(3.3 ± 0.7)e–7
081024B	0	5	1.64 ± 0.47	5.6/5	(4.0 ± 3.0)e–7
–	0	1	2.0 ± 0.7		
–	1	5	1.65 ± 0.8		
090217	0	100	2.22 ± 0.4	4/5	(4.0 ± 3.3)e–7
090323	0	400	2.05 ± 0.2	6/10	(7.9 ± 4.0)e–7
–	0	200	2.16 ± 0.3		
–	200	400	1.98 ± 0.23		
090328	0	100	1.76 ± 0.35	8.8/10	(1.2 ± 0.2)e–7
–	100	200	1.61 ± 0.23		
–	200	400	1.81 ± 0.25		
090510	0	7	2.15 ± 0.1	23/30	(4.7 ± 1.0)e–6
–	0.1	0.324	1.8 ± 0.25		
–	0.324	1.05	2.28 ± 0.23		
–	1.05	6.12	2.22 ± 0.28		
090626	0	600	1.7 ± 0.12	8/10	(4.7 ± 1.0)e–8
–	0	70	1.6 ± 0.3		
–	70	170	1.99 ± 0.33		
–	170	600	1.65 ± 0.3		
090902B	0	320	2.32 ± 0.16	6/10	(1.8 ± 0.3)e–6
–	4	6	2.67 ± 0.64		
–	6	9	2.34 ± 0.51		
–	9	10.5	2.5 ± 0.43		
–	10.5	12.5	2.37 ± 0.47		
–	12.5	21	1.92 ± 0.27		
–	21	40	1.76 ± 0.28		
–	40	80	1.84 ± 0.3		
–	80	160	1.73 ± 0.52		
–	160	320	1.91 ± 0.44		
090926A	0	25	2.34 ± 0.14	4/10	(1.7 ± 0.3)e–6
–	2	8	2.75 ± 0.5		
–	8	15	2.36 ± 0.22		
–	15	25	2.0 ± 0.23		
–	25	75	1.85 ± 0.22		
–	75	225	2.09 ± 0.42		
091003	0	100	1.85 ± 0.25	12/7	(7.4 ± 1.2)e–8
–	100	200	1.81 ± 0.4		
–	200	400	1.8 ± 0.2		

Note. We give the time interval (t_0-t_1) for the accumulation of each spectrum, the photon index, the flux integrated between 100 MeV and 100 GeV and the *C*-statistic for degrees of freedom (d.o.f.). Errors are given at the 90 per cent confidence level.

We have analysed the *Fermi*–LAT data[1] with the *Fermi* SCIENCE-TOOLS (V9R15P2) released on 2009 August 8. LAT count light curves (extracted with the GTBIN tool) were rebinned in time with a variable bin size, different for each burst.

We analysed the spectrum of the emission detected by the LAT. For the brightest part of the burst, we applied the standard procedure (i.e. extracted the spectra and created the relative response files with the GTBIN and GTRSPGEN tools, respectively). We considered the spectrum over a time interval covering entire light curve, and if the burst was particularly bright we also extracted the spectrum over a time interval coincident with the duration of the emission as observed by the GBM. To verify if and at what extent the LAT spectrum could vary with time, we extracted a series of consecutive spectra for each burst. As in most bursts we did not find evidence

for substantial spectral evolution of the LAT component, we used the average spectrum to convert the count rate into physical units.

3 RESULTS

Light curves. Fig. 1 shows the light curves obtained from the selection of the LAT events with energies >0.1 GeV. In each plot, we also show the time interval (hatched region) corresponding to the duration of the GBM light curve (T_{90} in Table 1). In 9/11 events, there is a peak in the LAT light curve and the latter has a duration much longer than the duration of the GBM light curve (shown by the hatched region in Fig. 1). After the peak, the light curves of different GRBs show a similar temporal decay. In a few cases (see also Ghirlanda et al. 2010), a rising of the light curve as t^2 is seen before the peak. The three faintest GRBs (GRB 090323, GRB 090328 and GRB 090626) have light curves that appear much flatter than the other ones (please note the different scale of their *y*-axis), and we

[1] http://fermi.gsfc.nasa.gov/ssc/data/
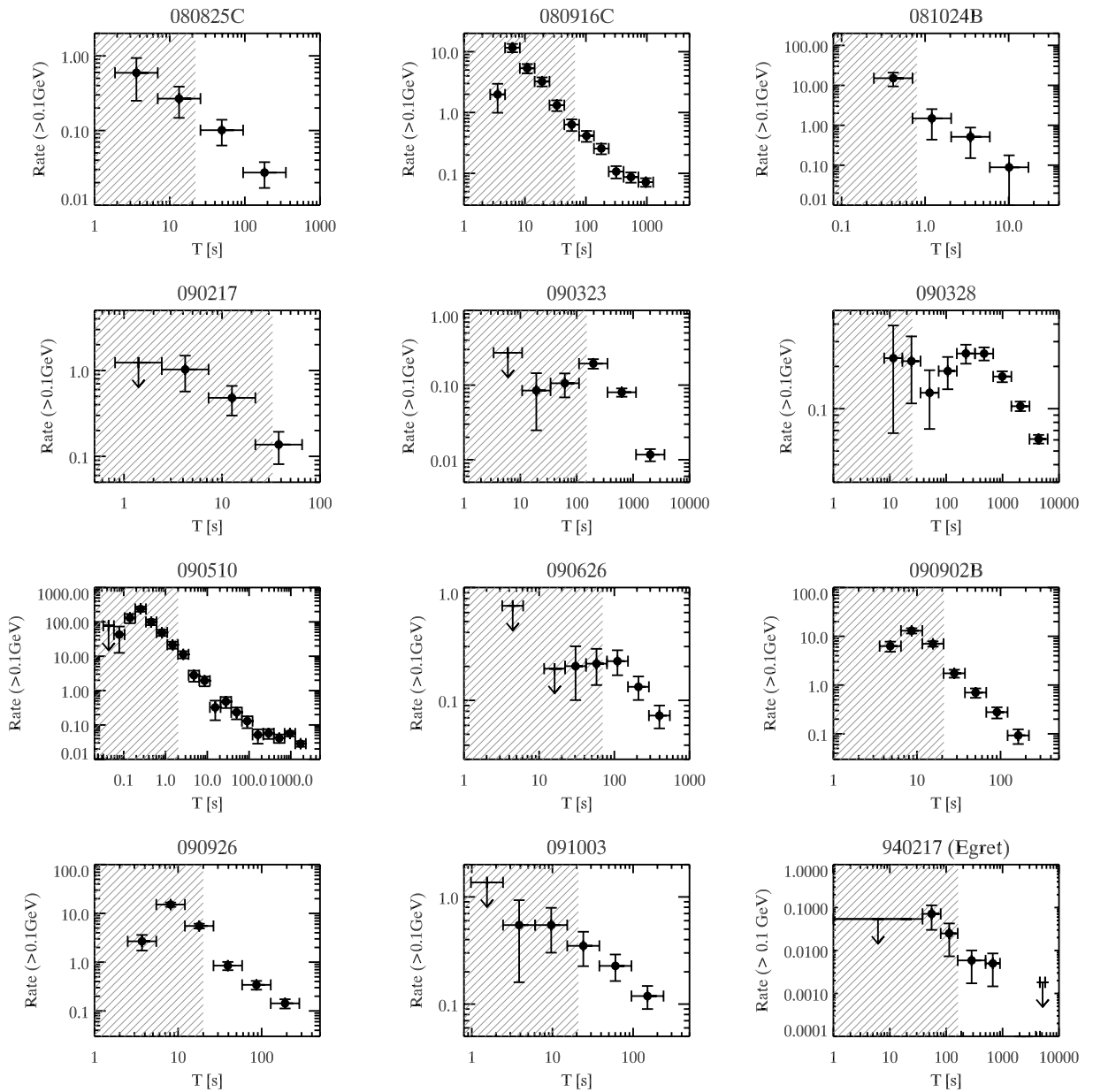
Figure 1. Light curves of the 11 GRBs detected by LAT plus GRB 940217, as detected by EGRET (bottom-right panel). The hatched region represents the duration (T_{90}) of the emission detected by the GBM in the 8 keV–40 MeV energy range (for GRB 940217, it refers to the emission detected by BATSE). Times are in the observer frame for all bursts and arrows represent 2σ upper limits.

cannot exclude that the background, in these cases, plays some role. The bottom-right panel shows the light curve of GRB 940217 as detected by EGRET (Hurley et al. 1994), selecting photons above 100 MeV. As can be seen, also this burst show a similar decaying light curve.

Spectral evolution. In Table 2, we report the results of the LAT spectral analysis. For each burst, the first line refers to the spectrum used to convert the count rate into physical units while the following lines give the spectral index for each time resolved spectrum. We report in Table 2 also the flux integrated between 100 MeV and 100 GeV. By comparing the time-resolved spectral results of individual bursts we see that there is no evidence of strong spectral evolution of the LAT spectral index during the burst. On average, all the spectral index are distributed between 1.5 and 2.2.

Spectral slopes in the LAT versus GBM. In Fig. 2, we compare the spectral index of the LAT emission with the spectral index of the average GBM spectrum (whose spectral parameters are reported in Table 1). The low-energy spectral index α (circles in Fig. 2, red in the electronic version) of the Band model (or of the cut-off power-law model for GRB 081024B and GRB 090323) is systematically harder than the spectral index of the LAT component. The high-energy spectral index β of the Band model (open squares in Fig. 2, blue in the electronic version) appears softer than the LAT spectrum. An extreme case is GRB 090902B which clearly shows that the LAT component is spectrally different from the tail of the Band function. Indeed, in this burst there is also evidence of a soft spectral excess detected in the GBM below 50 keV (Abdo et al. 2009c; de Palma et al. 2009). We also note that in only two bursts, GRB 080916C
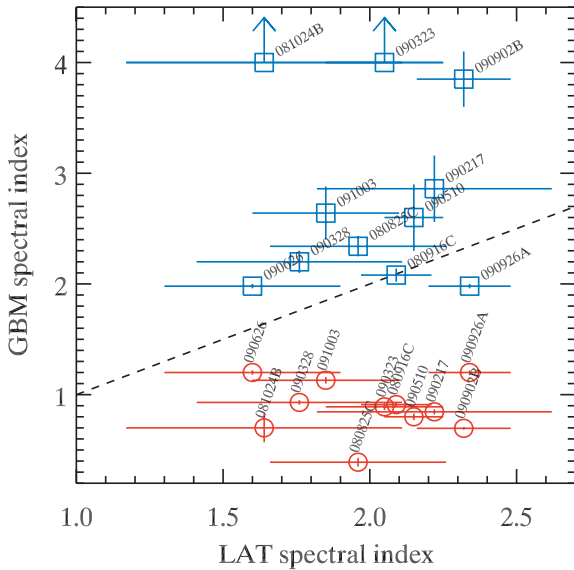
Figure 2. Spectral index (α and β, red circles and blue squares, respectively) of the GBM time-integrated spectra (reported in Table 1) versus the spectral index obtained from the analysis of the LAT data presented in this paper (Table 2). The dashed line represents equality. The two lower limits are GRB 081024B and GRB 090323 whose time-integrated GBM spectrum is best fitted by a cut-off power-law model. For illustrative purposes, we assumed $\beta > 4$ for these two bursts. This plot shows that the LAT spectrum is harder than the low-energy spectral index of the Band model fitting the GBM spectrum (red circles) and it is harder than the high-energy spectrum of the Band model fitting the GBM spectrum (blue squares).

(Abdo et al. 2009a) and GRB 090926, the high-energy spectrum of the Band model is consistent with the spectral slope of the LAT data.

LAT versus GBM fluences. Fig. 3 shows the fluence in the LAT energy range 100 MeV–100 GeV (using the fluxes listed in Table 2) as a function of the fluence in the GBM energy range 8 keV–10 MeV. The shaded regions correspond to 1σ–3σ of the distribution of GBM fluences for the 121 GRBs detected so far by the GBM with measured prompt phase emission peak energy (Nava et al., in preparation) and that appeared in the GRBs Coordinate Network (GCN) circulars.[2] The dashed line marks equality between the two fluences. We can see that all but the two short bursts (GRB 081024B and GRB 090510) have GBM fluences much brighter than average. If all GRBs with GBM fluences 1σ brighter than average and in the LAT field of view (i.e. one half) were detected by the LAT, we should have a fraction of LAT-detected GRBs of $\sim$16 per cent, which is not far from the actual fraction (see also Guetta & Pian 2009). One can compare Fig. 3 with fig. 4 of Le & Dermer (2009), showing the pre-*Fermi* bursts detected by EGRET and BATSE. Apart from GRB 930131, showing an EGRET fluence comparable to the BATSE one, all the other pre-*Fermi* GRBs seem to be characterized by a fainter GeV fluence relative to their fluence at smaller energies, but the sample is too small to draw any conclusion.

Time decay of the LAT flux. We converted the count rate of Fig. 1 into luminosity. For the bursts without measured redshifts, we assumed a typical redshift of 2 for long events, while for GRB 081024B we used a redshift of 1. We show the light curves of eight GRBs with good-quality data in the top panel of Fig. 4, where the times are in the source rest frame. The grey shaded stripe has a
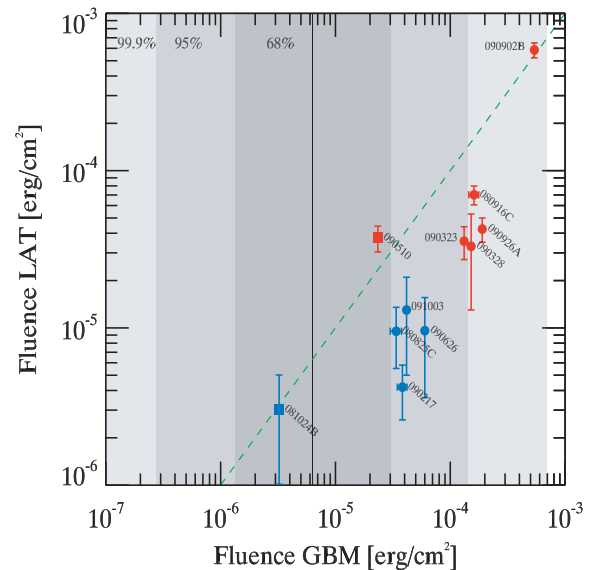
Figure 3. Fluence in the 0.1–100 GeV LAT energy range as a function of the 8 keV–10 MeV GBM ones. Short GRBs are marked with filled squares, long GRBs with filled circles. GRBs with known redshifts are the ones with a LAT fluence larger than 2×10^{-5} erg cm^{-2} (red in the electronic version). The shaded areas indicate the 1σ–3σ values of the distribution of fluences of the 121 GRBs with E_{peak} (as of 2009 October) detected by the GBM.

slope of $t^{-10/7}$, and it is shown for comparison. We can see that the light-curves show a power-law behaviour, and that the decay slope is often steeper than unity. Initially, some bursts show a rising phase and therefore it is possible to define the peak time of their high-energy emission. As seen below, if the peak time marks the onset of the afterglow emission it can be used to estimate the bulk Lorentz factor Γ.

Common decay for the brightest LAT bursts. The bottom panel of Fig. 4 shows the light curves of the four brightest GRBs with redshift, once the 0.1–100 GeV luminosity is divided by the energetics $E_{\gamma,\text{iso}}$ of the flux detected by the GBM. The shaded stripe has a slope $t^{-10/7}$, and it is shown for comparison. These four GRBs show a common behaviour, being all consistent, within the errors, with the same decay, both in slope and in normalization. Note that GRB 090510, a short burst, behaves similarly to the other three bursts that belong to the long class, but its light curve begins much earlier. If we divide the light curves by the average luminosities as derived by the GBM [instead of the energetics; i.e. we multiply by the time $T_{90}/(1 + z)$] the resulting light curves of the four GRBs spread within a larger region.

To conclude, we find that (i) the LAT fluxes decay as power laws; (ii) the spectral shape at high energies is not strongly evolving; (iii) the LAT spectrum has a slope intermediate between the low- and high-energy slope (i.e. α and β) of the Band function used to fit the GBM data; and (iv) the brightest four GRBs show a common $t^{-1.5}$ decay and even the same normalization, once their LAT luminosities are divided by the GBM energetics.

These characteristics are the same as observed/predicted by the external shock scenario giving rise to the afterglow. We therefore suggest that the high-energy emission of the GRBs detected by the LAT has an afterglow origin. The fact that the high-energy emission overlaps in time with the prompt phase as seen in the GBM can be explained by invoking a relatively large value of the bulk Lorentz factor, corresponding to relatively small deceleration
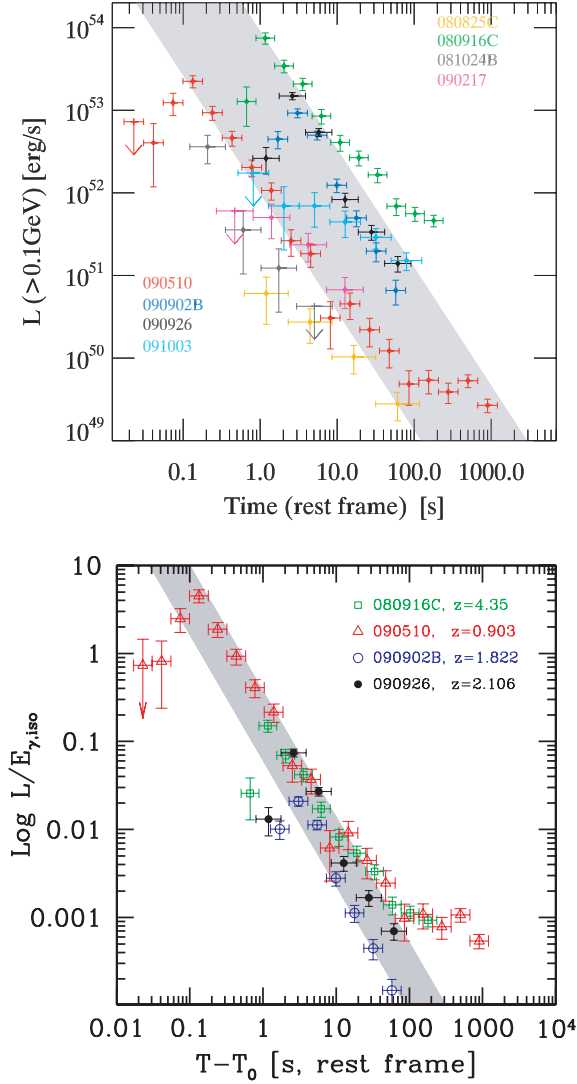
Figure 4. Top panel: light curves of the eight brightest bursts GRBs detected by LAT. The luminosities are integrated in the 0.1–100 GeV energy range at the source rest frame. For GRBs without measured redshifts, we assumed $z = 1$ for short and $z = 2$ for long events. The time is in the rest frame of the sources. Upper limits are at the 2σ level. The grey stripe indicates a slope $t^{-10/7}$. Bottom panel: light curves of the four brightest GRBs with redshift, normalized to the total energetics of the GBM energetics. The luminosities are integrated in the 100 MeV–100 GeV energy range at the source rest frame. For GRBs without measured redshifts, we assumed 1 for short and 2 for long events. The time is in the rest frame of the sources. Upper limits are at the 2σ level. The yellow stripe indicates a slope $t^{-10/7}$.

radii and onset times largely contracted by the Doppler effect. What is at odd with respect to the 'standard afterglow scenario is the relatively steep slope of the flux decay, even when the high-energy spectrum indicates that we are observing this component close to its spectral peak. We offer a solution to this problem in the next section, where we will also argue that the likely emission process producing the high-energy flux is synchrotron radiation.

4 THE BOLOMETRIC AFTERGLOW LUMINOSITY

In the early afterglow phases, the emission is likely to occur in the *fast cooling* regime, in which all the energy of the accelerated

electrons is radiated away. In this case, the bolometric afterglow luminosity can be calculated in a simple way. Assume that the shock generated by the fireball has reached a radius R, and that it moves within a region characterized by a uniform number density n (this case can be easily generalized to different density radial profiles). The (comoving) emitting volume is $V' = 4\pi R^2 \Delta R'$, since we are assuming that the fireball is a spherical shell. The radiative cooling rate of the electrons is measured by $\dot{\gamma}$ where $\gamma m_e c^2$ is the electron energy, and the emitting particles are distributed in energy according to $N(\gamma)$. Note that the time derivative, the electron energies and their energy distribution are all measured in the comoving frame. In this case, the bolometric luminosity is

$$L_{\rm iso} = \Gamma^2 m_e c^2 \int V' N(\gamma) \dot{\gamma}\, d\gamma$$
$$= 4\pi R^2 \Gamma^2 m_e c^2 \int N(\gamma) \dot{\gamma} \Delta R'(\gamma)\, d\gamma$$
$$= 4\pi R^2 \Gamma^2 m_e c^3 \int N(\gamma) \gamma\, d\gamma. \quad (1)$$

We have used the fact that the distance $\Delta R'$ can be approximated by the cooling length as measured in the comoving frame: $\Delta R'(\gamma) = ct'_{\rm cool} = c\gamma/\dot{\gamma}$. Therefore, $\Delta R'$ is energy dependent; it is smaller for high-energy particles that spend most of their energy faster. Equation (1) is remarkably *independent of the specific radiation process*. The integral in equation (1) must correspond to the fraction ϵ_e of the available energy density as measured in the comoving frame, i.e.

$$m_e c^2 \int N(\gamma) \gamma\, d\gamma = \epsilon_e n \Gamma^2 m_p c^2. \quad (2)$$

Therefore, equation (1) becomes

$$L_{\rm iso} = 4\pi R^2 \Gamma^4 m_p c^3 \epsilon_e n$$
$$= 16\pi a^2 t^2 \Gamma^8 m_p c^5 \epsilon_e n, \quad (3)$$

where we have assumed that the size R is measured by the observed time as $R = 2act\Gamma^2$. The factor a is equal to 1 if the fireball moves at a constant speed, and becomes greater than 1 when it decelerates (see e.g. Sari 1997). Equation (3) is valid as long as the afterglow is in the fast cooling regime, irrespective of the radiative or adiabatic nature of the process that changes only the relation between the observed time t and the bulk Lorentz factor Γ at that time. In fact, when the forward shock is coasting (i.e. before being notably decelerated) we have $L_{\rm iso} \propto t^2$ in both cases. When the shock starts to decelerate, the observed luminosity decreases according to the appropriate $\Gamma(t)$ function, which is different for the adiabatic and radiative cases.

Adiabatic case. We adopt the following relation between the observed time and Γ:

$$\Gamma^8 = \frac{3E_{\rm k,f}}{32\pi a^3 n m_p c^5 t^3}, \quad (4)$$

where $E_{\rm k,f}$ is the kinetic energy of the fireball after the prompt phase. The same equation can be used to define the deceleration time $t_{\rm dec}$, once we set $a = 1$ and substitute Γ_0 to Γ. If η is the efficiency of conversion of the initial kinetic energy $E_{\rm k,0}$ into radiation of the prompt phase, we have

$$E_{\rm k,f} = E_{\rm k,0} - E_{\gamma,\rm iso} = E_{\gamma,\rm iso}\left(\frac{1-\eta}{\eta}\right). \quad (5)$$

When the fireball is still in its coasting phase, the observed luminosity increases as t^2 due to the increased visible area. After $t_{\rm dec}$,

the observed luminosity decreases as t^{-1}, as can be seen inserting equation (4) into equation (3):

$$L_{\mathrm{iso,a}} = 16\pi t^2 \Gamma_0^8 m_\mathrm{p} c^5 \epsilon_\mathrm{e} n; \qquad t \ll t_{\mathrm{peak}}$$

$$L_{\mathrm{iso,a}} = \frac{3}{2a}\frac{\epsilon_\mathrm{e} E_{\mathrm{k,f}}}{t}; \qquad t \gg t_{\mathrm{peak}}$$

$$t_{\mathrm{peak,a}} = \left(\frac{3E_{\mathrm{k,f}}}{32\pi a \Gamma_0^8 n m_\mathrm{p} c^5}\right)^{1/3} = \frac{t_{\mathrm{dec}}}{a^{1/3}}$$

$$t_{\mathrm{dec}} \equiv \left(\frac{3E_{\mathrm{k,f}}}{32\pi \Gamma_0^8 n m_\mathrm{p} c^5}\right)^{1/3}. \tag{6}$$

To find t_{peak}, we equated the two expressions for L_{iso}.

Radiative case. In this case, an important fraction of the dissipated energy is radiated away. This implies that the emitters, i.e. the electrons, receive a large fraction of the available energy (directly or through the interactions with protons, and/or through reconnection of the magnetic field) and radiate it efficiently. In this case, the energy of the fireball decreases, changing the $\Gamma(t)$ function. This has been studied by Blandford & McKee (1976); and the solution is (Katz & Piran 1997; Vietri 1997; Sari, Piran & Narayan 1998)

$$\Gamma = \frac{(\Gamma_0+1)(X+1)^2 + (\Gamma_0-1)}{(\Gamma_0+1)(X+1)^2 - (\Gamma_0-1)}$$

$$X = \frac{m}{M_\mathrm{f}} = \frac{4\pi\Gamma_0 m_\mathrm{p} n c^2 R^3}{3E_{\mathrm{k,f}}} \tag{7}$$

where M_f is the mass of the fireball and m is the swept interstellar mass. When the fireball is decelerating, but still relativistic, $X \ll 1$ and equation (7) simplifies to

$$\Gamma \sim \frac{1}{X} = \left(\frac{3E_{\mathrm{k,f}}}{32\pi\Gamma_0 m_\mathrm{p} n c^5 a^3 t^3}\right)^{1/7} = \Gamma_0 \frac{t_{\mathrm{dec}}^{3/7}}{a^{3/7}} t^{-3/7}. \tag{8}$$

Inserting this into equation (3), we obtain

$$L_{\mathrm{iso,r}} = 16\pi t^2 \Gamma_0^8 m_\mathrm{p} c^5 \epsilon_\mathrm{e} n; \qquad t \ll t_{\mathrm{peak}}$$

$$L_{\mathrm{iso,r}} = \frac{3\epsilon_\mathrm{e} E_{\mathrm{k,f}}}{2a^{10/7}} t_{\mathrm{dec}}^{3/7} t^{-10/7} \qquad t \gg t_{\mathrm{peak}}$$

$$t_{\mathrm{peak,r}} = \frac{t_{\mathrm{dec}}}{a^{5/12}}. \tag{9}$$

The peak time of the bolometric afterglow emission (estimated equating the two limiting forms of L_{iso}) precedes the deceleration time by a small factor. Integrating $\mathrm{d}R = 2c\Gamma^2 \mathrm{d}t$ assuming $\Gamma \propto t^{-3/8}$ (adiabatic) or $\Gamma \propto t^{-3/7}$ (radiative) we have $a = 4$ or 7 for the adiabatic and radiative cases, respectively. Therefore, $t_{\mathrm{peak}} = 0.63\, t_{\mathrm{dec}}$ (adiabatic) and $t_{\mathrm{peak}} = 0.44 t_{\mathrm{dec}}$ (radiative).

After the peak time, radiative afterglows decrease faster than adiabatic ones, as the fireball energy is no longer constant, but decreases. As noted by Sari et al. (1998), partially radiative fireballs would have scalings intermediate between the pure adiabatic and pure radiative limits. Even if, initially, a fireball is purely radiative, after some time it must become adiabatic, as a consequence of incomplete cooling of the accelerated electrons. If the electrons are accelerated above some minimum energy $\gamma_\mathrm{m} m_\mathrm{e} c^2$, this will occur when this electrons cannot cool in a dynamical time, so when $\gamma_\mathrm{m} = \gamma_\mathrm{c}$, where $\gamma_\mathrm{c} m_\mathrm{e} c^2$ is the energy of those electrons cooling in $t' \sim \Gamma t \sim R/(ac\Gamma)$.

When observing the flux in a particular frequency range $\Delta\nu$, we are never observing the bolometric flux, so in general the time decays are different from t^{-1} (adiabatic) or $t^{-10/7}$ (radiative). If the emitted spectrum (in a νF_ν plot) has a peak at ν_{peak}, and ν_m decreases in time, then the time decay would be flatter for $\nu < \nu_{\mathrm{peak}}$ and steeper for $\nu > \nu_{\mathrm{peak}}$. However, if the observed flux has a spectral index close to unity (i.e. $\nu \sim \nu_{\mathrm{peak}}$) then the observed flux

becomes a good proxy for the bolometric one, with the same time decay slope.

For a uniform circumburst medium, the relation between the decay slope α and the spectral index β for a flux density $F(\nu, t) \propto t^{-\alpha} \nu^{-\beta}$ is (Sari et al. 1998)

$$\alpha = \frac{2}{7}(6\beta - 1) \tag{10}$$

returning $\alpha = 10/7 = 1.43$ when $\beta = 1$ and $\alpha = 1.77$ for $\beta = 1.2$. This derivation assumes that the number of accelerated electrons is always a fixed fraction of the protons present in the circumburst medium.

5　PAIR-ENRICHED INTERSTELLAR MEDIUM

When the prompt phase emission spectrum extends above $E_{\mathrm{peak}}(1+z) \sim m_\mathrm{e} c^2$, we can convert a fraction of the high-energy photons into electron–positron pairs. This case has been studied in detail by Thompson & Madau (2000), Mészáros, Ramirez-Ruiz & Rees (2001) and especially by Beloborodov (2002).

The basic idea is that although the scattering depth of the circumburst medium can be much smaller than unity, it can nevertheless scatter a fraction of the prompt phase photons along non-radial directions. These scattered photons can then interact with the arriving high-energy prompt phase photons producing pairs. The process *is not* controlled by the probability of the interaction between the scattered and the primary prompt phase photons: this is almost unity (up to very large distances), due to the huge amount of prompt phase photons. The process is controlled by how many photons are scattered. The full description of this scenario is rather complex, and we refer to Beloborodov (2002) for the complete treatment. We focus here on a few estimates, to give an idea of the importance of the process. The basic quantity of interest is the number of scatterings done by a single electron located at a distance R from the emission site of the prompt phase emission. Using the Thomson cross-section for simplicity, and setting $h\nu \equiv x m_\mathrm{e} c^2$, this number is

$$N_{\mathrm{sc}} = \sigma_\mathrm{T} \frac{E_{\gamma,\mathrm{iso}}}{\langle x \rangle m_\mathrm{e} c^2 4\pi R^2 c t_{\mathrm{burst}}} c t_{\mathrm{burst}} \sim 640 \frac{E_{\gamma,\mathrm{iso},54}}{\langle x \rangle R_{16}^2}. \tag{11}$$

Almost all these photons will be converted into pairs immediately after they have been scattered. This implies that the circumburst medium will be greatly enriched by pairs before the arrival of the forward shock. This can occur even if the total number of intercepted photons is a tiny fraction of the total. For instance, if the interstellar medium is homogeneous with density n, the total number of scattered photons within 10^{17} cm is only a fraction $\tau_\mathrm{T} = 6.65 \times 10^{-8}\, n$ of the total number of photons of the prompt phase. But, this is enough to greatly pair-enrich the circumburst medium. Furthermore, the scattering and the pair production processes pre-accelerate the interstellar medium. If there is one proton per primary electron, and if the energy deposited by the single scattering with subsequent pair production is roughly equal to $m_\mathrm{e} c^2$, this process will be important below a certain distance, below which there occur more than 1000 scatterings for a primary electron (i.e. in this case the proton associated with the primary electron will start to move with $\Gamma \sim 2$ in the radial direction). As a feedback, if the medium starts to move then the typical energy of the scattered photons will start to decrease, quenching off the pair-production process (i.e. the scattered photons have too small energies to interact with photons around a few MeV). On the other hand, the produced pairs, if they are re-isotropized in a short time, can also scatter the incoming prompt phase radiation, enhancing the process and making it exponential.

Therefore, equation (3) is only a simple but rough estimate of a much more complex scenario. We can nevertheless draw some important conclusions.

(i) Pairs are important if the prompt phase emission extends the above threshold.

(ii) At a negligible expense (i.e. the fraction of absorbed prompt phase emission is negligible), the environment is largely enriched by pairs.

(iii) The distance for which the number of produced pairs equals the number of primary electrons is sufficiently large and affects the properties of the forward shock up to some relevant observed time. For instance, the 'closure' relation given by equation (3) is modified as long as the number of pairs per proton is larger than unity, because in this case the energy $\gamma_m \propto \Gamma \, n/n_+ \propto \Gamma \, R^2$. Here, n_+ is the pair density. Introducing this extra R^2 dependence, we find

$$\alpha = \frac{2}{7}(4\beta + 1) \qquad (12)$$

returning $\alpha = 10/7 = 1.43$ when $\beta = 1$ and $\alpha = 1.66$ for $\beta = 1.2$.

(iv) Although the details of the shock acceleration process are controversial, it is reasonable to assume that the ratio of the energy given to leptons and protons will increase, if we have many leptons per proton. This is then one way to have a radiative fireball.

We therefore propose that bursts whose prompt phase emission extends above $m_e c^2$ should be characterized by an early radiative (then powerful) afterglow.

5.1 Additional processes

We consider here other processes that can be relevant for the formation of the high-energy afterglow.

(1) When $t_{\text{bursts}} > t_{\text{dec}}$, the region of the forward shock where leptons are accelerated is illuminated by the flux of the prompt phase emission (of luminosity $L_{\gamma,\text{iso}}$). This component lasts as long as the forward shock is illuminated by the prompt phase (see Beloborodov 2005a). The corresponding energy density, as measured in the comoving frame of the forward shock, is

$$U'_{\text{ext}} = \frac{L_{\gamma,\text{iso}}}{4\pi R^2 c \Gamma^2} \qquad (13)$$

where the subscript 'ext' stands for 'external' to the afterglow emitting region. This has to be compared with the local magnetic energy density

$$U'_B = \epsilon_B n m_p c^2 \Gamma^2. \qquad (14)$$

Therefore, the ratio between the synchrotron and the 'external Compton' (i.e. the luminosity produced by scattering U'_{ext}) luminosities is (see also Beloborodov 2005a)

$$\frac{L_{\text{EC}}}{L_{\text{syn}}} = f \frac{U'_{\text{ext}}}{U'_B} = \frac{f \, L_{\gamma,\text{iso}}}{4\pi R^2 \Gamma^4 \epsilon_B n m_p c^3} = 0.18 \frac{f \, L_{\gamma,\text{iso},53}}{R_{17}^2 \Gamma_3^4 \epsilon_{B,-1} n}. \qquad (15)$$

The factor $f < 1$ accounts for the suppression of the power emitted in the direction of the observer due to the anisotropic pattern of the incoming photons in the frame of the fireball. An order of magnitude estimate of its value can be gained through a simple example. In the frame of the fireball, assume that all the seed photons for the scattering are coming radially. Electrons travelling at $\theta' = 180°$ from the photons lose energy at a rate $\propto \gamma^2 (1 - \beta \cos \theta') \sim 4\gamma^2$. Electrons moving at $90°$ lose energy at a rate $\propto \gamma^2$. This is the emission that the observer (on the Earth) will preferentially see. Therefore, the factor f is less than, but of the order of, unity. This external Compton

component would start to be important at frequencies above $\nu_{\text{EC}} \sim \gamma_m^2 \nu_{\text{peak}} \sim \gamma_{m,3}^2 \nu_{\text{peak,MeV}}$ TeV. Below ν_{EC}, we should have $F(\nu) \propto \nu^{-1/2}$.

(2) The high-energy emission can also be produced by the synchrotron self-Compton (SSC) process (see e.g. Corsi, Guetta & Piro 2009; Fan et al. 2008), particularly important when (i) $\epsilon_e > \epsilon_B$; (ii) we are in the fast cooling regime; and (iii) we are in the Thomson limit (i.e. the scattering can be described by the Thomson cross-section).

Conditions (i) and (ii) are always fulfilled in radiative fireballs, while condition (iii) may be violated. The limit for the Thomson regime can be derived considering the dimensionless frequency $x'_m = h\nu_m/(\Gamma \, m_e c^2)$ (as measured in the comoving frame) and the electron energy γ_m. The entire process occurs in the Klein–Nishina regime if $x'_m \gamma_m > 1$, i.e. when

$$\Gamma^3 \epsilon_e^3 \epsilon_B^{1/2} n^{1/2} \left[\frac{m_p}{m_e} \frac{n}{n_+} \right]^3 > 1.77 \times 10^{14}. \qquad (16)$$

For moderate pair production (i.e. $n_+/n \lesssim 100$) and for still large Γ, the early SSC process is then in the Klein–Nishina regime, and is therefore inefficient. Furthermore, the SSC spectrum starts to be important at ν_{SSC} given by

$$\nu_{\text{SSC}} \sim \gamma_m^2 \nu_m \sim 7 \times 10^{22} \epsilon_e^4 \epsilon_B^{1/2} n^{1/2} \Gamma_3^6 \left[\frac{m_p}{m_e} \frac{n}{n_+} \right]^4 \text{ Hz.} \qquad (17)$$

It is a strong function of n/n_+: for fewer than 100 pairs per proton (and still a large Γ), the SSC spectrum starts at frequencies above the LAT range (with a flux reduced by Klein–Nishina effects). The middle panel of Fig. 5 shows ν_{SSC} as a function of time for one particular case.

We conclude that the most likely radiation process originating the LAT emission is synchrotron.

To illustrate the above considerations and to give an example of the predicted high-energy flux in radiative fireballs, we have calculated the bolometric flux emitted in one specific case, assuming that the prompt phase energetics $E_{\gamma,\text{iso}} = 10^{53}$ erg, $\eta = 0.2$, $z = 1$, $\Gamma_0 = 1000$, $n = 1 \text{ cm}^{-3}$, $p = 2$. Furthermore, we assumed a duration of 1 s and $\epsilon_e = 0.9$, $\epsilon_B = 0.1$. The resulting bolometric luminosity (normalized to $E_{\gamma,\text{iso}}$) is shown in the top panel of Fig. 5, together with its corresponding energetics [$E_{\text{bol}}(t) = \int_0^t L_{\text{bol}}(t')dt'$]. We also indicate the t^{-1} and the $t^{-10/7}$ time behaviour (dashed black lines). The middle panel shows the time profile of three characteristic frequencies: the injected frequency ν_m; the cooling frequency ν_c; and the SSC frequency $\nu_{\text{SSC}} \equiv \gamma_m^2 \nu_m$ [see also Beloborodov (2005b) for the case of pair enriched circumburst material, but with an adiabatic fireball].

The two upper shaded areas correspond to the frequency ranges covered by the LAT and GBM, while the lower one indicates the optical frequency range. The bottom panel shows the time profile of the minimum Lorentz factor of the injected electron γ_m, the cooling Lorentz factor γ_c, the bulk Lorentz Γ, together with the time profile of the magnetic field B, and the number of pairs per proton n_+/n, calculated according to equation (11). This quantity is crucial to calculate γ_m, since the same available energy must be divided by the total number of leptons, including the pairs. Since their amount changes with R (and correspondingly with the observed time), the time profile of γ_m is greatly modified by the presence of pairs. As a consequence, both ν_m and ν_{SSC} are largely affected, their values being much lower than in the absence of pairs. Note a caution: although the presence of pairs may be crucial to bring the process to the radiative regime, the exact amount of pairs
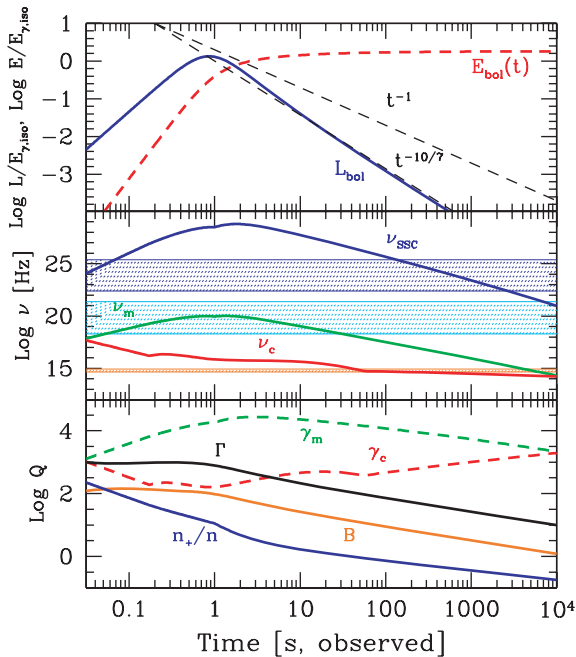
Figure 5. Top panel: time profiles of the bolometric luminosities and the corresponding cumulative energetics, in units of the initial kinetic energy of the fireball. For this particular example, we have assumed a radiative fireball with $z = 1$, $E_{\gamma,\text{iso}} = 10^{53}$ erg, $\eta = 0.2$, $T_{90} = 1$s, $\Gamma_0 = 10^3$, $\epsilon_e = 0.9$ and $p = 2$. The circumburst medium is homogeneous with density $n = 1\,\text{cm}^{-3}$. The dashed lines corresponds to t^{-1} and $t^{-10/7}$, i.e. the adiabatic and radiative cases. Pair production is accounted for in a approximated way, assuming that all scattered photons are transformed into pairs, but assuming that there are at most m_p/m_e pairs per primary electron. Middle panel: the time profiles of the frequencies ν_m, ν_c and $\nu_{\text{SSC}} \equiv \gamma_m^2 \nu_m$. The hatched areas mark the energy ranges of the LAT instrument (0.1–100 GeV), the GBM instrument (8–1000 keV) and the optical range (corresponding to the U and R filters). Bottom panel: the time profiles of the injected energy γ_m and the cooling energy γ_c. We also show the profile of Γ, of the magnetic field B (assuming $\epsilon_B = 0.1$), and the number of pairs per primary electron n_+/n. Since $n = 1$, this also corresponds to the density of pairs.

is difficult to calculate, being partially dependent on the exact shape and time evolution of the spectrum of the prompt phase emission above threshold, the presence or not of a magnetic field embedded in the circumburst medium, a possible clumping of this medium and so on. Ours are bound to be only rough estimates. Bearing the above caveat in mind, we find that the synchrotron emission, at the peak time, should have a flux $F(\nu) \propto \nu^{-0.5}$ between ν_c and ν_m and $F(\nu) \propto \nu^{-p/2}$ (equal to ν^{-1} in this example) up to $\nu_{\text{max}} = \nu_m(\gamma_{\text{max}}/\gamma_m)^2$. Therefore, $\gamma_{\text{max}}/\gamma_m \gtrsim 10^3$ ensures that the synchrotron emission extends up to the GeV range.

Note that the $\nu^{-p/2}$ part of the spectrum may start in the GBM energy range, depending on the exact amount of pairs. There is then the possibility that the afterglow emission 'contaminates' the prompt phase emission seen by the GBM. In some cases, this 'contamination' can appear as an excess at both extremes of the GRB energy range, especially if pairs are very important, decreasing γ_m (as in the case of GRB 090902B, Abdo et al. 2009c). Also the opposite (i.e. the prompt phase 'contaminates' the afterglow seen in the LAT) can occur, especially when the high-energy Band index β is not too soft. In this latter case, most of the prompt phase photons contributing to the LAT flux should be at low energies.

For simplicity, we have assumed that ϵ_e is constant, and not proportional to the amount of pairs per proton (since this number

Table 3. Parameters for the radiative afterglow models.

GRB	Γ_0	$E_{\gamma,\text{iso}}$	η	n (cm^{-3})	p
Fig. 5	1000	1.0e53	0.2	1	2
080916C	900	5.6e54	0.32	2	2
090510	2000	5.0e52	0.13	0.1	2.1
090902B	630	4.4e54	0.25	2	2.6
090926	670	2.0e54	0.14	3	2.5

is uncertain). However, the radiative phase should end in any case when γ_c becomes greater than γ_m since in this case most of the energy given to electrons cannot be radiated away in a dynamical time.

6 APPLICATION TO SPECIFIC BURSTS

We applied the radiative scenario to the four brightest (in the LAT) GRBs with redshift. They are the same as illustrated in Fig. 4, namely GRB 080916C, GRB 090510, GRB 090902B and GRB 090926. In principle, the number of parameters used for the adopted model is limited (they are listed in Table 3), but we adopted a few rather drastic simplifications.

(i) We consider the fireball, when colliding with the interstellar medium, as 'thin'. In other words, we assume that it can act as a piston having a total energy $E_{k,f}$. This is completely right for short GRBs, but not for long ones. According to Fig. 1, the *Fermi*–LAT emission of several GRBs starts while the emission seen by the GBM has not ended. In this case, the t^2 rising behaviour of the LAT light curve can be different (see Sari 1997).

(ii) When calculating the number of pairs produced by the circumburst medium, we neglect the amplification (exponential) effect of the produced pairs that can themselves scatter the incoming radiation. The momentum deposited in the circumburst medium is also taken into account only by imposing that the maximum number of pairs per proton is m_p/m_e, since a larger number correspond to a mildly relativistic motion of the medium and the quenching-off of the pair-producing mechanism. For simplicity, we use the Thomson cross-section for scattering, and assume that most of the prompt phase photons are close to the threshold for pair production.

(iii) We assume that *all* electrons and positrons are accelerated. If, instead, only a fraction of them receive the entire available energy then the typical Lorentz factors of the accelerated leptons are larger.

(iv) We use a fixed value of ϵ_e, even if the number of pairs populating the circumburst medium decreases with R. Consequently, we use the radiative solution all throughout the shown evolution, with no transition to the adiabatic case.

Bearing in mind these caveats, Figs 6–9 show the light curves of the four GRBs interpreted on the basis of our radiative model, with the main parameters listed in Table 3. In the cases of GRB 080916C and GRB 090510, we have also added a constant flux to the light curve, to account for the presence of the background, flattening off the observed light curves. In the case of GRB 090510, the fact that the flux above 200 s is due to the background has been confirmed by De Pasquale et al. (2009, see their fig. 1). Also for 080916C the points above 1000 s are affected by background (see Abdo et al. 2009a, and their fig. 4). So, for these two bursts, the flattening of the light curve at late times should not be due to the contribution of the SSC component entering in the LAT energy range (as predicted
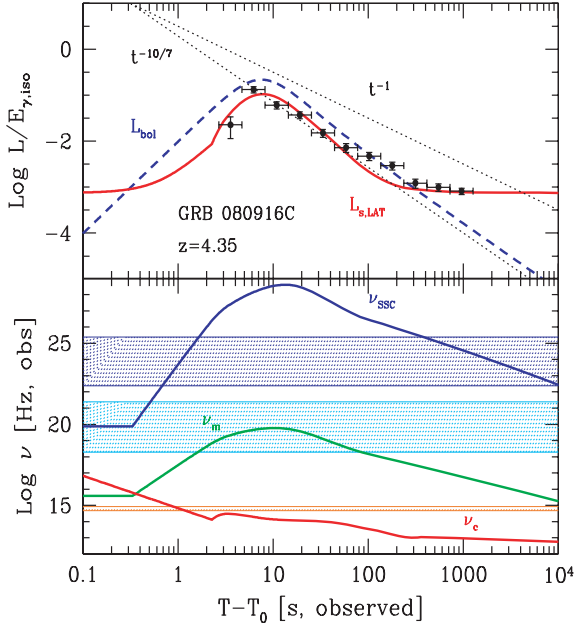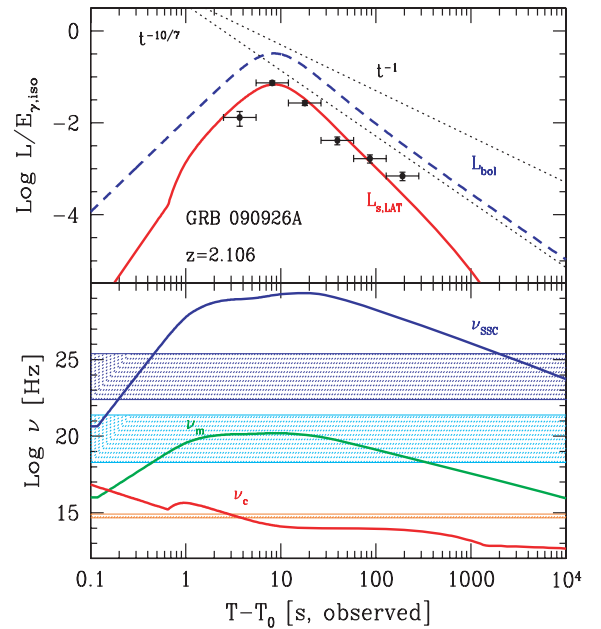
Figure 6. The long burst GRB 080916C. Parameters are listed in Table 3.
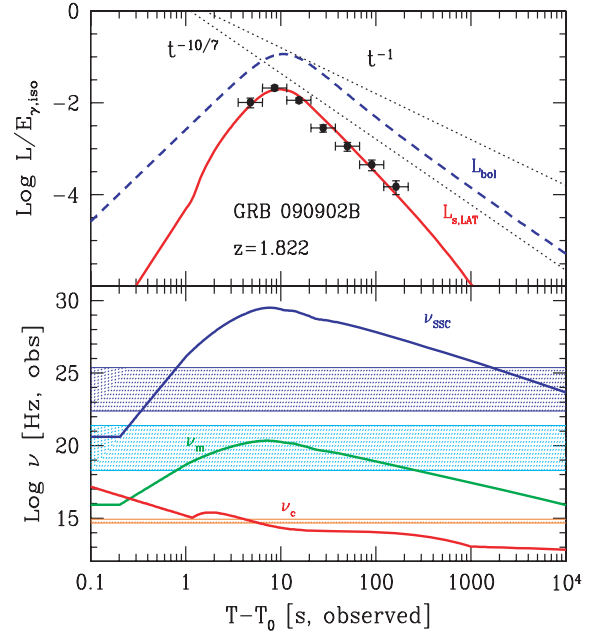
Figure 8. The long burst GRB 090902. Parameters are listed in Table 3.
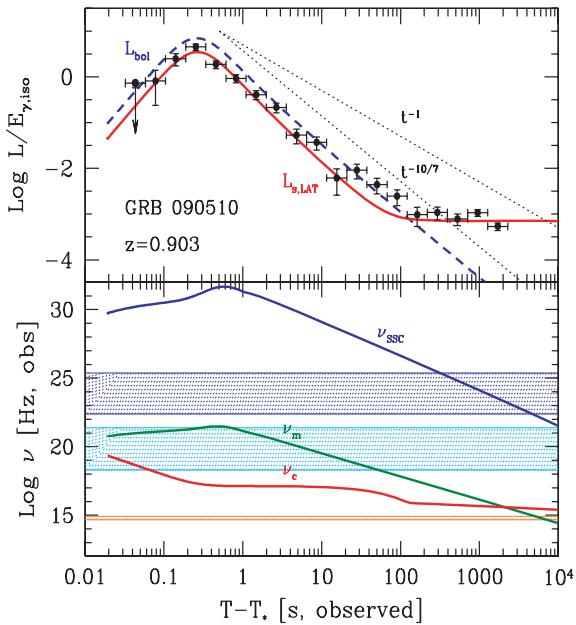
Figure 7. The short burst GRB 090510 assuming $T_* = 0.6$ s. Parameters are listed in Table 3.

Figure 9. The long burst GRB 090926. Parameters are listed in Table 3.

by Dermer, Chiang & Mitman 2000, and tantalizingly suggested by Figs 6 and 7), but only because we did not subtract the background.

The solid lines shown in all top panels refer to the luminosity integrated in the 0.1–100 GeV energy range, while the dashed thick lines are the bolometric fluxes (both normalized to the prompt phase energetics of each burst). For comparison, we show also the lines corresponding to t^{-1} and to $t^{-10/7}$. We can see that in all cases the radiative interpretation is in good agreement with what observed, and that in all cases the predicted ν_m is well below the 0.1 GeV value. This ensures that in the LAT we should see a spectral shape $F(\nu) \propto \nu^{-p/2}$. The observed decay slope and the spectral index in the LAT energy range (see Table 1) are consistent with equation (3),

but the errors on $\beta = \Gamma_{LAT} - 1$ are too large to use this as a reliable test.

7 DISCUSSION

The bulk Lorentz factors found are in the range 630–900 for the long bursts, and 2000 for the short GRB 090510. We believe that these relatively large values are the key to understanding why only a minority of bursts are detectable by the LAT. A large bulk Lorentz factor, in fact, means an early peak time of the afterglow (see equations 6 and 9), and this in turn means a large flux. *Faster fireballs have brighter afterglows*. This is true for adiabatic as well as radiative fireballs. If the emission occurs in the radiative regime then the

afterglow will be brighter still, since all the energy dissipated in the external shock is radiated away.

If the circumburst medium is enriched by electron–positron pairs, we have a more favourable set up for a radiative process. If the acceleration mechanism divides its energy to all particles then leptons should receive a total energy exceeding the one given to protons. But, this may be only one of the means to have a radiative fireball. An alternative is to have a strong coupling between electrons and protons, with an efficient energy flow from protons to electrons. In any case, we can easily test if pairs are indeed important by simply comparing the general properties of the early afterglow for bursts of different E_{peak} and high-energy index β, since only those bursts whose prompt phase photon energies exceed $m_e c^2$ should efficiently populate the circumburst medium by pairs. As an example, we may test if the high-energy emission is present only in GRBs of high E_{peak} (in the rest frame) as it appears to be the case until now or if it occurs also for bursts with a small E_{peak}. If this will occur, and if the flux will decay with a slower rate than $t^{-10/7}$ then we will have an indication of a fast fireball that emits adiabatically because of no pair enrichment of the circumburst medium. In other words, a possible test of the idea of having radiative afterglows because of pair enrichment is to find a different time decay for the high-energy emission in classical GRBs whose prompt phase emission extends to high energies and X-ray flashes, characterized by relatively small values of E_{peak}.

The radiative interpretation could ease the efficiency problem of the afterglow phase. This problem concerns the ratio of the energetics emitted during the prompt and afterglow phases, which is much larger than unity (e.g. Zhang et al. 2007). According to the standard internal/external shock scenario, one expects the opposite since external shocks should be much more efficient than internal ones to dissipate the kinetic energy of the fireball. These estimates were based on the observed X-ray afterglow energetics (see e.g. Willingale et al. 2007; Ghisellini et al. 2009), and we can now revise them including the much more powerful high-energy gamma-ray emission, bringing the total afterglow energetics to be roughly equal to the prompt phase one. Furthermore, if the fireball is indeed radiative in the first phases, with a consequent fast decay, we can understand why the afterglow emission at later times and at other frequencies is so faint.

According to our findings, bursts detected by the LAT may be the ones with the largest Γ, and can be used to explore the high-end Γ-distribution. On the other hand, one can wonder about the possibility to detect with the LAT bursts with relatively smaller Γ, smaller high-energy luminosities and with light curves peaking at larger peak times. Even if rare, nearby objects with these properties might be still detectable, offering a direct way to test our ideas, even if they should be characterized by much lower peak luminosities in the LAT, they should have LAT/GBM fluence ratios similar to those presented in this paper, and lower values of Γ.

One of the arguments put forward against the afterglow interpretation of the high-energy flux is its variability, which according to Abdo et al. (2009c) can have a time-scales Δt_{var} as short as 90 ms. If true, this is certainly a severe problem for the afterglow interpretation. On the other hand, the knowledge of Δt_{var} is limited by the small number of received photons. When the entire light curve, lasting for a few hundred seconds, is composed of a few hundred events, one can define a very short Δt_{var} only if there is an exceptional 'bunching' of photons in contiguous time-bins, and we do not see it in the bursts we analysed.

Finally, we would like to emphasize the importance of establishing, in general, if the high- and low-energy emissions are produced by the same electrons at the same time or instead if they are produced by different electrons at different times. As the study of GRB 090510 (Abdo et al. 2009b; Ghirlanda et al. 2010) has demonstrated, we are reaching the required data quality to put strong constraints on the theories predicting the violation of the Lorentz invariance at small scales, which can be tested by comparing the possible delay of the *arrival* times of high-energy photons. The critical issue about these studies is to know exactly the *generation* time of the high-with respect to low-energy emission. Therefore, it becomes crucial to establish if the flux received by the LAT is the extension in energy of the prompt phase emission or if it is afterglow radiation.

REFERENCES

Abdo A. A. et al., 2009a, Sci, 323, 1688
Abdo A. A. et al., 2009b, Nat, 462, 331
Abdo A. A. et al., 2009c, ApJ, 706, L138
Atwood W. B. et al., 2009, ApJ, 697, 1071
Beloborodov A. M., 2002, ApJ, 565, 808
Beloborodov A. M., 2005a, ApJ, 618, L13
Beloborodov A. M., 2005b, ApJ, 627, 346
Blandford R. D., McKee C. F., 1976, Phys. Fluids, 19, 1130
Bissaldi E., 2009, GCN 9933
Bissaldi E., Connaughton V., 2009, GCN 9866
Chaplin V., van der Horst A. J., Preece R., 2008, GCN 8682
Corsi A., Guetta D., Piro L., 2009, A&A, preprint (arXiv:0905.1513)
de Palma F., Bissaldi E., Tajima H., Guiriec S., Omodei N., Vasileiou V., Connaughton V., 2009, GCN 9872
De Pasquale M. et al., 2009, ApJ, preprint (arXiv:0910.1629)
Dermer C. D., Chiang J., Mitman K. E., 2000, ApJ, 537, 785
Fan Y.-Z., Piran T., Narayan R., Da-Ming W., 2008, MNRAS, 384, 1483
Fishman G. J., Meegan C. A., 1995, ARA&A, 33, 415
Gao W.-H., Mao J.-R., Xu D., Fan Y.-Z., 2009, ApJ, 706, L33
Ghirlanda G., Ghisellini G., Nava L., 2010, A&A, submitted (arXiv:0909.0016)
Ghisellini G., Nardini M., Ghirlanda M., Celotti A., 2009, MNRAS, 393, 253
Guetta D., Pian E., 2009, in Proc. 7th Agile Meeting: The Bright Gamma-Ray Sky, in press (arXiv:0910.2134)
Guiriec S., Connaughton V., Briggs M., 2009, GCN 9336
Hurley K. et al., 1994, Nat, 372, 652
Kaneko Y., Gonzalez M. M., Preece R. D., Dingus B. L., Briggs M. S., 2008, ApJ, 677, 1168
Katz J. I., Piran T., 1997, ApJ, 490, 772
Kumar P., Barniol-Duran R., 2009, Nat, preprint (arXiv:0905.2417)
Le T., Dermer C. D., 2009, ApJ, 700, 1026
McEnery J., the *Fermi* LAT team, 2008, GCN 8684
Meegan C. et al., 2009, ApJ, 702, 791
Mészáros P., Ramirez-Ruiz E., Rees M. J., 2001, ApJ, 554, 660
Ohno M., Cutini S., McEnery J., Chiang J., Koerding E., van der Horst A., 2009, GCN 9021
Omodei N., 2008, GCN 8407
Preece R., 2008, GCN 8678
Rau A., 2009, GCN 9983
Rau A., Connaughton V., Briggs M., 2009, GCN 9057
Razzaque S., Dermer C. D., Finke J. D., 2009, ApJ, preprint (arXiv:0908.0513)

Sari R., 1997, ApJ, 489, L37
Sari R., Piran T., Narayan R., 1998, ApJ, 497, L17
Thompson C., Madau P., 2000, ApJ, 538, 205
van der Horst A. J., Connaughton V., 2008, GCN 8141
van der Horst A. J., Goldstein A., 2008, GCN 8278
Vietri M., 1997, ApJ, 488, L105
von Kienlin A., 2009a, GCN 8902
von Kienlin A., 2009b, GCN 9579

Willingale R. et al., 2007, ApJ, 662, 1093
Zhang B., Peer A., 2009, ApJ, 700, L65
Zhang B. et al., 2007, ApJ, 655, 989
Zou Y.-C., Fan Y.-Z., Piran T., 2009, MNRAS, 396, 1163

This paper has been typeset from a TEX/LATEX file prepared by the author.